Thermodynamic Control in Ion Radical Cleavages through Out-of-Cage Diffusion of Products. Dynamics of C−C Fragmentation in Cation Radicals of *tert*-Butylated NADH Analogues and Other Ion Radicals

Agnès Anne, Sylvie Fraoua, Jacques Moiroux,* and Jean-Michel Savéant*

Contribution from the Laboratoire d'Electrochimie Moléculaire de l'Université Denis Diderot (Paris 7), 2 place Jussieu, 75251 Paris Cedex 05, France

Received December 18, 1995[⊗]

Abstract: According to the nature of the alkyl group, cation radicals of NADH analogues alkylated para to the nitrogen atom (AHR), generated by direct or indirect electrochemical means, may undergo C−C fragmentation or deprotonation. The former reaction is dominant with the *tert*-butyl substituent and the latter with methyl and phenyl substituents. It is shown that the cleavage reaction produces AH^+ and the *tert*-butyl radical which is then rapidly oxidized to form the *tert*-butyl cation. Changing the A group allows a variation of the C−C fragmentation rate constant (determined by cyclic voltammetry or redox catalysis) by *ca.* six orders of magnitude for a change of *ca.* 0.4 eV in the standard free energy of the reaction. The logarithm of the rate constant varies linearly with the standard free energy of the reaction with a slope of 1/(60 meV) showing that fragmentation is kinetically controlled by the diffusion of the two fragments out of the solvent cage rather than by activation. The kinetic data thus allow an easy determination of the thermodynamics of the fragmentation. Analysis of previous rate data concerning an extended series of bibenzylic cation and anion radicals shows that they follow the same behavior.

The chemistry of cation radicals often involves deprotonation and carbon−carbon fragmentation.[1] However, relatively few time-resolved studies have been reported for deprotonation[2−11] and even fewer for carbon−carbon fragmentation.[12,13]

One goal of the work described below was to investigate the dynamics of carbon−carbon fragmentation in cation radicals of alkylated NADH analogues attempting to relate kinetic reactivity to the thermodynamic driving force. It has been previously shown that $BNAHC(CH_3)_3^{\bullet+}$ (see Chart 1) undergoes expulsion of the *tert*-butyl radical (reaction 1) rather than deprotonation (reaction 2) even in the presence of strong bases.[14]

$$AHR^{\bullet+} \rightleftharpoons AH^+ + R^\bullet \quad (1)$$

$$AHR^{\bullet+} + B \rightleftharpoons AR^\bullet + BH^+ \quad (2)$$

Conversely, with $MAHCH_3^{\bullet+}$, $MAHPh^{\bullet+}$ (as well as with their deuterated analogues),[9d] and with $MAHC_2H_5^{\bullet+}$ and $MAHCH_2CO_2C_2H_5^{\bullet+}$ [10b] deprotonation (dedeuteration) always appeared faster than C−C fragmentation. With $MAHCH_2Ph$,[•+ 9d,10b] $MAHCHPh_2^{\bullet+}$, $MAHCH(CH_3)_2^{\bullet+}$, and $MAHCH(CH_3)CO_2C_2H_5^{\bullet+}$ [10b] both deprotonation and C−C fragmentation were observed, while with $MAHC(CH_3)_3^{\bullet+}$, the latter reaction predominated.[15]

In the present work, we took as illustrative examples the four *tert*-butyl derivatives shown in Chart 1 to investigate the dynamics of C−C fragmentation in cation radicals.

Results

C−C Fragmentation vs Deprotonation. Cyclic voltammetric and preparative-scale evidence that $BNAHC(CH_3)_3^{\bullet+}$ undergoes C−C fragmentation rather than deprotonation has been provided in a previous publication.[14a] Figure 1 shows the cyclic voltammograms of $BQAHC(CH_3)_3$, $BQCNHC(CH_3)_3$, and $MAHC(CH_3)_3$ at low scan rate where the oxidation wave is irreversible. In all three cases, a one-electron irreversible peak

[⊗] Abstract published in *Advance ACS Abstracts,* April 1, 1996.

(1) (a) For a recent review, see: ref 1b. (b) Albini, A.; Mella, M.; Freccero, M. *Tetrahedron* **1994**, *50*, 575.

(2) (a) Schlesener, C. J.; Amatore, C.; Kochi, J. K. *J. Am. Chem. Soc.* **1984**, *106*, 7472. (b) Schlesener, C. J.; Amatore, C.; Kochi, J. K. *J. Phys. Chem.* **1986**, *90*, 3747. (c) Masnovi, J. M.; Sankararaman, S.; Kochi, J. K. *J. Am. Chem. Soc.* **1989**, *111*, 2263.

(3) Bacciochi, E.; Del Giacco, T.; Elisei, F. *J. Am. Chem. Soc.* 1**993**, *115*, 12290.

(4) Dinnocenzo, J. P.; Banach, T. E. *J. Am. Chem. Soc.* **1989**, *111*, 8646.

(5) (a) Xu, W.; Mariano, P. S. *J. Am. Chem. Soc.* **1991**, *113*, 1431. (b) Xu, W.; Zhang, X.; Mariano, P. S. *J. Am. Chem. Soc.* **1991**, *113*, 8863. (c) Zhang, X.; Yeh, S. R.; Hong, S.; Freccero, M.; Albini, A.; Mariano, P. S. *J. Am. Chem. Soc.* **1994,** *116*, 4211.

(6) (a) Reitstöen, B.; Parker, V. D. *J. Am. Chem. Soc.* **1990**, *112*, 4968. (b) Parker, V. D.; Chao, Y.; Reitstöen, B. *J. Am. Chem. Soc.* **1991**, *113*, 2336. (c) Parker, V. D.; Tilset, M. *J. Am. Chem. Soc.* **1991**, *113*, 8778.

(7) (a) Ci, X.; Kellett, M. A.; Whitten, D. G. *J. Am. Chem. Soc.* **1991**, *113*, 3893. (b) Leon, J. W.; Whitten, D. G. *J. Am. Chem. Soc.* **1993**, *115*, 8038.

(8) For deprotonation of cation radicals of NADH analogues see refs. 9−11.

(9) (a) Hapiot, P.; Moiroux, J.; Savéant, J.-M. *J. Am. Chem. Soc.* **1990**, *112*, 1337. (b) Anne, A.; Hapiot, P.; Moiroux, J.; Neta, P.; Savéant, J.-M. *J. Phys. Chem.*. **1991**, *95*, 2370. (c) Anne, A.; Hapiot, P.; Moiroux, J.; Neta, P.; Savéant, J.-M. *J. Am. Chem. Soc.* **1992**, *114*, 4694. (d) Anne, A.; Fraoua, S.; Hapiot, P.; Moiroux, J.; Savéant, J.-M. *J. Am. Chem. Soc.* **1995**, *117*, 7412.

(10) (a) Fukuzumi, S.; Kondo, Y.; Tanaka, T. *J. Chem. Soc., Perkin Trans. 2* **1984**, 673. (b) Fukuzumi, S.; Tokuda, Y.; Kitano, T.; Okamoto, T.; Otera, J. *J. Am. Chem. Soc.* **1993**, *115*, 8960.

(11) Sinha, A.; Bruice, T. C. *J. Am. Chem. Soc.* **1984**, *106*, 7291.

(12) Sankararaman, S.; Perrier, S.; Kochi, J. K. *J. Am. Chem. Soc.* **1989**, *111*, 6448.

(13) (a) Maslak, P.; Asel, S. L. *J. Am. Chem. Soc.* **1988**, *110*, 8260. (b) Maslak, P.; Chapman, W. H. *J. Chem. Soc., Chem. Commun.* **1989**, 1810. (c) Maslak, P.; Chapman, W. H. *Tetrahedron* **1990**, *46*, 2715. (d) Maslak, P.; Narvaez, J. N. *Angew. Chem., Int. Ed. Engl.* **1990**, *29*, 283. (e) Maslak, P.; Chapman, W. H. *J. Org. Chem.*. **1990**, *55*, 6334. (f) Maslak, P.; Vallombroso, T. M.; Chapman, W. H.; Narvaez, J. N. *Angew. Chem., Int. Ed. Engl*. **1994**, *33*, 73.

(14) (a) Anne, A.; Moiroux, J.; Savéant, J.-M. *J. Am. Chem. Soc.* **1993**, *115*, 10224. (b) This observation was then used as a probe in the discussion of the mechanism of hydride transfer in NADH analogues.[14a]

(15) In ref 10b, R^+ and $AH^\bullet$ are viewed as the primary products of C−C fragmentation of the cation radical. However, as discussed later on, there is a considerable driving force advantage for the other mode of fragmentation forming $R^\bullet$ and AH^+ (reaction 1).

0002-7863/96/1518-3938$12.00/0

Chart 1

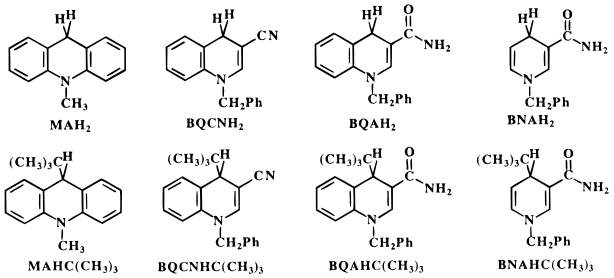

is observed upon scan reversal which has exactly the same location as the one-electron irreversible cathodic peak of pure samples of $BQAH^+$, $BQCNH^+$, and MAH^+, respectively. These cathodic peaks cannot be confused with those of the corresponding *tert*-butylated cations, since, as observed with $BNAC(CH_3)_3^+$, the latter are shifted by more than 200 mV in the negative direction as compared to the AH^+ cations. With $BQAHC(CH_3)_3$ and $BQCNHC(CH_3)_3$ the same behavior was found with other bases, having pK_as ranging from 9.4 to 15.6, with concentrations ranging from 10 to 40 mM, in unbuffered or buffered conditions. In the case of $BQAHC(CH_3)_3$, the formation of $BQAH^+$ was confirmed by preparative-scale electrolysis (1 mM substrate in acetonitrile + 0.1 M NEt_4BF_4 in the presence of 3,5-dimethylpyridine, pK_a = 14.7) using cyclic voltammetric and HPLC identification.

With $MAHC(CH_3)_3$, the formation of MAH^+ was observed with bases having pK_as ranging from 9.4 to 15.4, with concentrations ranging from 10 to 300 mM, in unbuffered or buffered conditions. With bases of higher pK_a, starting with 2,4,6-trimethylpyridine (pK_a = 15.6), the cation radical of $MAHC(CH_3)_3$ still loses the *tert*-butyl group but also the methyl group borne by the nitrogen, resulting in quantitative formation of acridine

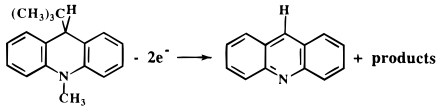

as revealed by preparative-scale electrolysis. The same reaction was also observed to occur with the same bases upon laser pulse irradiation in the presence of CCl_4 used as an oxidative quencher for triggering the formation of the cation radical.[9b] The mechanism of this double fragmentation reaction is not known at present and shall be the object of further investigations.[16]

Mechanism and Kinetics of C−C Fragmentation. Two modes of C−C fragmentation may be envisaged:

$$AHR^{\bullet+} \rightleftharpoons AH^+ + R^\bullet \qquad (1)$$

$$AHR^{\bullet+} \rightleftharpoons AH^\bullet + R^+ \qquad (1')$$

In terms of standard free energies, $\Delta G^0_{(1)} - \Delta G^0_{(1')} = E^0_{AH^+/AH^\cdot} - E^0_{R^+/R^\cdot}$, reaction 1 has a strong advantage over reaction 1′, $\Delta G^0_{(1)} - \Delta G^0_{(1')}$ (eV) = −1.195 (A = BNA), −0.810 (A = BQA), −0.610 (A = BQCN), −0.555 (A = MA) as derived from the previously determined values of $E^0_{AH^+/AH^\cdot}$[9c] and the oxidation potential of the *tert*-butyl radical, 0.09 V vs SCE.[17]

Once $R^\cdot$ is formed, it is immediately oxidized by a second molecule of $AHR^{\cdot+}$ since the standard potential of the $AHR^{\cdot+}/AHR$ couple (Table 1) is much more positive than the standard potential of the $C(CH_3)_3^+/C(CH_3)_3^\cdot$ couple. The $C(CH_3)_3^+$ cation thus produced then reacts rapidly with the solvent and/or residual water (with $BNAHC(CH_3)_3^{\cdot+}$, the main product was indeed found to be *tert*-butyl alcohol[14a]). The reaction mechanism thus consists in the following three successive steps.

$$AHR^{\bullet+} \overset{k_1}{\rightleftharpoons} AH^+ + R^\bullet \qquad (1)$$

$$R^\bullet + AHR^{\bullet+} \overset{k_2}{\rightleftharpoons} R^+ + AHR \qquad (2)$$

$$R^+ + \text{solvent and/or residual water} \overset{k_3}{\rightleftharpoons} \text{products} \qquad (3)$$

With $MAHC(CH_3)_3^{\cdot+}$, C−C fragmentation is not too fast. The standard potential of the $MAHC(CH_3)_3^{\cdot+}/MAHC(CH_3)_3$ couple could thus be derived from the cyclic voltammograms of $MAHC(CH_3)_3$ at a classical 1 mm-diameter gold disk microelectrode where reversibility was reached above 20 V/s (Figure 2). Reversible cyclic voltammograms could also be obtained with $BQAHC(CH_3)_3$ and $BQCNHC(CH_3)_3$ but only at a 17 μm-

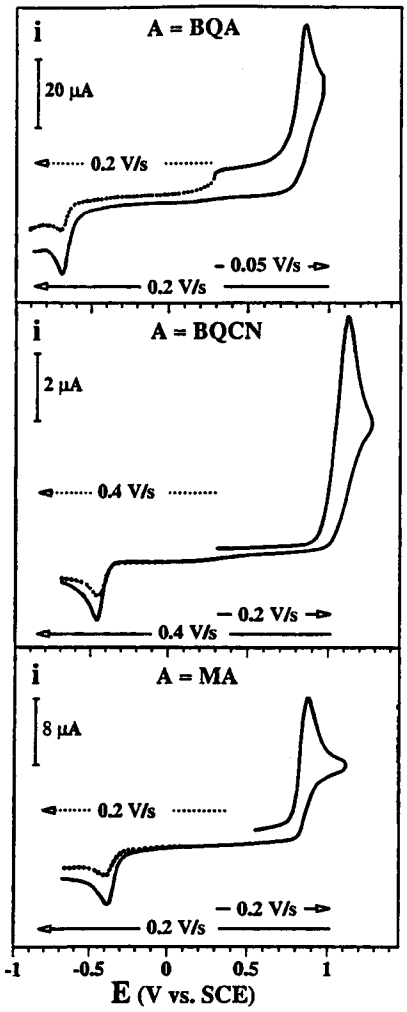

Figure 1. Cyclic voltammetry of $AHC(CH_3)_3$ and AH^+ in acetonitrile + 0.1 M NEt_4BF_4.

A	BQA	BQCN	MA
$[AHC(CH_3)_3]$ (mM)	1.4	1.0	1.7
$[AH^+]$ (mM)	0.2	0.22	0.22

(16) We already know that demethylation does not occur after the cleavage of the *tert*-butyl group has produced MAH^+ since we have found that pure samples of the latter compound are stable toward demethylation in the presence of the bases used in the present study.

Table 1. Standard free energies of reactions (1) and (2)

A	BNA	BQA	BQCN	MA
$E^0_{AHC(CH_3)_3^{\cdot+}/AHC(CH_3)_3}$ [a]	0.850	1.000	1.210	0.910
$\Delta G^0_{C(CH_3)_3^{\cdot}+AHC(CH_3)_3^{\cdot+}\rightarrow C(CH_3)_3^{+}+AHC(CH_3)_3}$ [b]	−0.760	−0.910	−1.120	−0.820
$\Delta G^0_{AH_2^{\cdot+}\rightarrow AH^{+}+H^{\cdot}}$ [b]	1.184	1.316	1.380	1.587
$\Delta G^0_{AHC(CH_3)_3^{\cdot+}\rightarrow AH^{+}+C(CH_3)_3^{\cdot}}$ [b]	0.129	0.223	0.297	0.496

[a] In V vs SCE. [b] In eV.

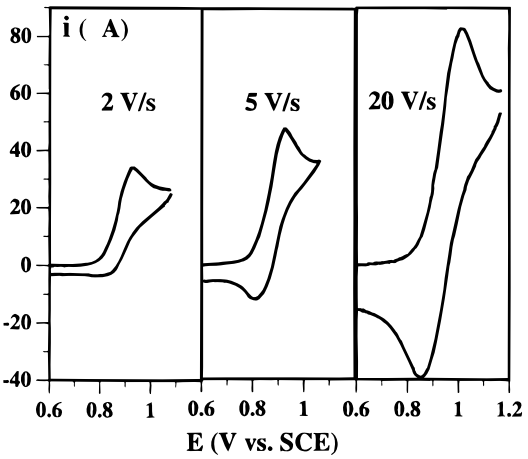

Figure 2. Cyclic voltammetry of $MAHC(CH_3)_3$ (2 mM) in acetonitrile + 0.1 M NEt_4BF_4 in the presence of 99.4 mM 3-methylpyridine (pK_a = 13.5). Temperature 20 °C.

diameter disk ultramicroelectrode[18b] where reversibility started to appear at 100 000 and 20 000 V/s, respectively. With $BNAHC(CH_3)_3^{\cdot+}$, C−C fragmentation is too fast for reversibility to be reached in the accessible range of scan rates. The standard potential was therefore derived from redox catalysis experiments as described further on. The standard potentials thus obtained are listed in Table 1. The ensuing values of the standard free energy of reaction 2 are all very negative justifying the assumption that the reaction is totally irreversible and has a rate constant equal to the diffusion limit ($k_2 = k_{dif} = 7.9\ 10^9\ M^{-1}\ s^{-1}$ [9c]).

A second thermodynamic factor is required for extracting the values of the rate constant k_1 from the experimental data, namely, the standard free energy of reaction 1. They were obtained as follows. The standard free energy $\Delta G^0_{AH_2^{\cdot+}\rightarrow AH^{+}+H^{\cdot}}$ for each A was first derived from the following equation, using previously determined values of the pK_a and of the standard potential of the $AH^+/AH^{\cdot}$ couple.[9] For $E^0_{H^+/H^{\cdot}}$, we used the most recent estimate (−2.012 V vs SCE in acetonitrile[19]).

$$\Delta G^0_{AH_2^{\bullet+}\rightarrow AH_+ + H_{\bullet}} = \frac{RT\ln 10}{F} pK_a, AH_2^{\bullet+} + E^0_{AH_+/AH_{\bullet}} - E^0_{H^+/H_{\bullet}}$$

$\Delta G^0{}_{AHR^{\cdot+}\rightarrow AH^{+}+R^{\cdot}}$ was then computed from the following equation

$$\Delta G^0_{AHR_{\bullet+}\rightarrow AH_+ + R_{\bullet}} = \Delta G^0_{AH_2^{\bullet+}\rightarrow AH_+ + H_{\bullet}} + \Delta G^{0,f}_{R^{\bullet}} - \Delta G^{0,f}_{H^{\bullet}} + \Delta G^{0,f}_{AH_2} - \Delta G^{0,f}_{AHR} + E^0_{AH_2^{\bullet+}/AH_2} - E^0_{AHR_{\bullet+}/AHR}$$

where the $\Delta G^{0,f}$s represent the free energies of formation of the subscript species from the elements. $\Delta G^{0,f}_{AH_2} - \Delta G^{0,f}_{AHR}$ was estimated by the Benson's incremental method, regarding the functional carbon as bound to two ethylenic carbons when A = BNA, one ethylenic and one benzenic carbon when A = BQA and BQCN, and two benzenic carbons when A = MA.[20] The free energies of formation of $H^{\cdot}$ and of $R^{\cdot}$ were obtained from ref 20. The ensuing values of $\Delta G^0_{AHC(CH_3)_3^{\cdot+}\rightarrow AH^{+}+C(CH_3)_3^{\cdot}}$ are listed in Table 1.

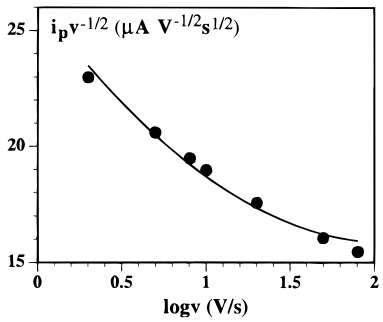

Figure 3. Cyclic voltammetry of $MAHC(CH_3)_3$ (2 mM) in acetonitrile + 0.1 M NEt_4BF_4 in the presence of 99.4 mM of 3-methylpyridine (pK_a = 13.5). Temperature 20 °C. Variation of the peak current with the scan rate (from 2 to 80 V/s). The solid line is the theoretical variation for log k_1 (s^{-1}) = 1.9 (see text).

As seen from the cyclic voltammograms of $MAHC(CH_3)_3$ in Figure 2, reversibility increases upon raising the scan rate, and, at the same time, the peak current passes from a value that corresponds to an electron stoichiometry that is larger than 1 to a value corresponding to 1. These variations of the peak current (i_p) are recast in Figure 3, under the form of a $i_p v^{-1/2}$ vs log v plot. It is seen that the best fitting with the theoretical variation is obtained for log k_1 (s^{-1}) = 1.9. The theoretical $i_p v^{-1/2}$ vs log v plots where computed for a reaction scheme including the electrode reaction below

$$AHR - e^- \rightleftharpoons AHR^{\bullet+}$$

and reactions 1−3 as depicted above. For the electrode reaction,

(17) (a) Wayner, D. D. M.; McPhee, D. J.; Griller, D. *J. Am. Chem. Soc.* **1988**, *110*, 132. (b) Most probably, the value of 0.09 V vs SCE is not exactly that of the standard potential of the $C(CH_3)_3^+/C(CH_3)_3^{\cdot}$ redox couple but rather an overall oxidation potential which is also a reflection of the kinetics of the electrode electron transfer (standard rate constant, k_S; transfer coefficient, α) and of the follow-up reaction of $C(CH_3)_3^+$ with the solvent and/or residual water. The later reaction is presumably very fast, making the electrode electron transfer the rate-determining step. Thus the steady-state half-wave potential may be expressed as (δ, thickness of the diffusion layer; D, diffusion coefficient): $E_{1/2} = E^0 - (RT/\alpha F)\ln(k_S\delta/D)$.[18a] Since $\alpha \approx 0.5$, $\delta \approx 10^{-2}$ cm, and $D \approx 10^{-5}\ cm^2\ s^{-1}$, $E^0(V) \approx 0.09 + 0.12\ \log[10^3 k_S(cm^{-1})]$. Although not accurately known, k_S should not be too different from 10^{-3} cm s^{-1}, taking into account solvent reorganization and the shortening of the C−C bonds from $C(CH_3)_3^{\cdot}$ to $C(CH_3)_3^+$. In such a case, $E^0 \approx E_{1/2}$. Even if this estimate of k_S is not very accurate, driving force advantage of reaction 1 over reaction 1′ is undoubtedly very large.

(18) (a) Andrieux, C. P.; Savéant, J.-M. Electrochemical Reactions. In *Investigations of Rates and Mechanisms of Reactions*; Bernasconi, C. F., Ed.; Wiley: New York, 1986; Vol. 6, 4/E, Part 2, pp 305−390. (b) Andrieux, C. P.; Hapiot, P.; Savéant, J.-M. *Chem. Rev.* **1990**, *90*, 723.

(19) (a) Parker, V. D. *J. Am. Chem. Soc.***1992**, *114*, 7458. (b) Parker, V. D. *J. Am. Chem. Soc.* **1993**, *115*, 1201 (erratum).

(20) Benson, S. N. *Thermodynamical Kinetics*; Wiley: New York, 1976.

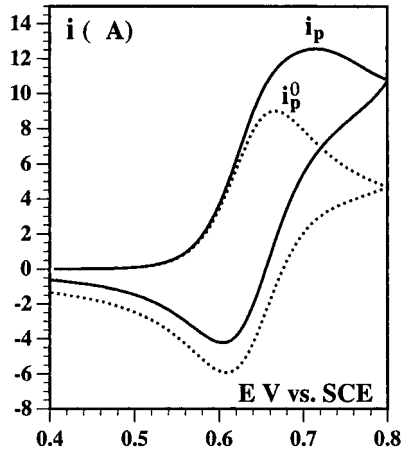

Figure 4. Cyclic voltammetry in acetonitrile + 0.1 M NEt_4BF_4 + 30 mM 3,5-dimethylpyridine ($pK_a = 14.7$) of acetylferrocene (4 mM) in the absence (dotted line) and presence (solid line) of $BQAHC(CH_3)_3$ (2 mM). Scan rate: 0.05 V/s.

the following values were used: standard potential 0.910 V vs SCE (Table 1), $k_S = 0.1$ cm s^{-1}, $\alpha = 0.5$. For K_1 we took the value, 4.5×10^{-9} M^{-1} s^{-1}, corresponding to the value of the standard free energy given in Table 1. Because it has a very large driving force (second row in Table 1), reaction 2 was regarded as irreversible with a rate constant equal to the diffusion limit, 7.9×10^9 M^{-1} s^{-1}.

These experiments and analyses were repeated with the same base in the presence of an equimolar amount of the conjugated acid as well as with other bases, namely, 2chloro- and 3-fluoroprydine ($pK_a = 6.3$ and 9.4, respectively) in unbuffered and buffered conditions at several concentrations ranging from 50 to 200 mM. Log k_1 was found to be the same within experimental error (log $k_1 = 1.9 \pm 0.1$), thus confirming the predominance of C−C fragmentation within this pH range.

Although reversibility could be reached in fast scan cyclic voltammetry for $BQAHC(CH_3)_3$ and $BQCNHC(CH_3)_3$, allowing the determination of the standard potentials, the current-potential responses did not prove of sufficient quality to safely derive the value of the C−C fragmentation rate constants. We therefore used the redox catalysis method instead. The principle of the method consists in oxidizing the substrate by the oxidized form, Q, of a redox couple, P/Q, generated at the electrode instead of direct oxidation by the electrode itself.[18] In the present case, the catalysis reaction scheme is as follows.

$$P - e^- \rightleftharpoons Q$$

$$Q + AHR \underset{k_{-0}}{\overset{k_0}{\rightleftharpoons}} P + AHR^{\bullet+} \qquad (0)$$

$$AHR^{\bullet+} \underset{k_{-1}}{\overset{k_1}{\rightleftharpoons}} AH^+ + R^{\bullet} \qquad (1)$$

$$R^{\bullet} + AHR^{\bullet+} \xrightarrow{k_{dif}} R^+ + AHR \qquad (2)$$

$$R^{\bullet} + Q \xrightarrow{k_{dif}} R^+ + P \qquad (2')$$

$$R^+ + \text{solvent and/or residual water} \xrightarrow{k_3} \text{products} \qquad (3)$$

Figure 4 shows a typical catalytic response obtained with $BQAHC(CH_3)_3$ and acetylferrocene ($E^0 = 0.638$ V vs SCE) as the catalyst. Starting from the reversible wave of the catalyst, addition of the substrate triggers an enhancement of the anodic peak and a partial loss of reversibility. The value of the ratio i_p/i_p^0 of the peak currents in the presence and absence of the substrate provides kinetic information on the set of reactions that follows the electrode P−Q reaction.[18]

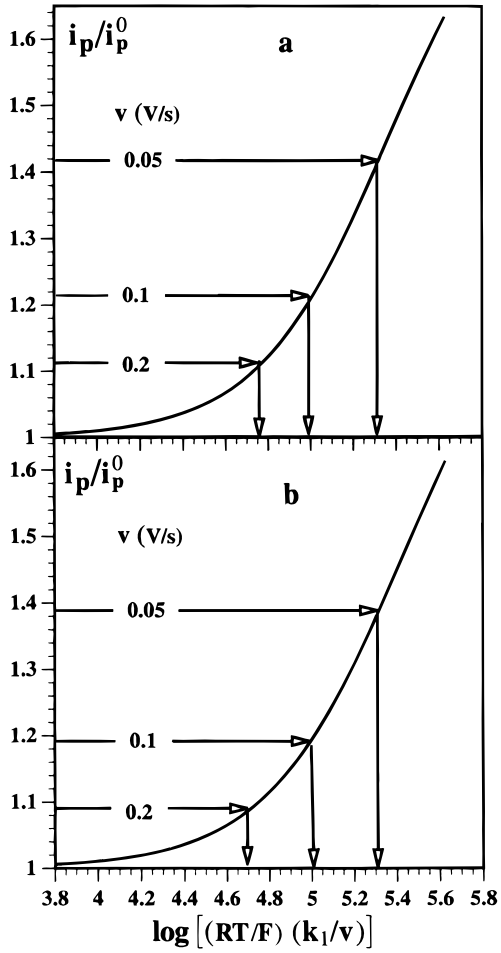

Figure 5. Cyclic voltammetry in acetonitrile + 0.1 M NEt_4BF_4 + 30 mM 3,5-dimethylpyridine ($pK_a = 14.7$) of acetylferrocene ($E^0_{cat} = 0.638$ V vs SCE) in the presence of $BQAHC(CH_3)_3$. Variation of the normalized catalytic peak current with the dimensionless rate parameter of reaction 1 (see text) and determination of k_1 at various scan rates. [acetylferrocene] = 10 (a) and 4 (b) mM. $[BQAHC(CH_3)_3] = 5.13$ (a) and 2.04 (b) mM.

Figure 5 illustrates the procedure we used for deriving the rate constant k_1 from the i_p/i_p^0 ratios obtained from cyclic voltammograms such as those represented in Figure 4. For each set of catalyst and substrate concentrations, the working curves, represented by the solid lines in Figure 5, were computed according to the reaction scheme above using the following values of the various equilibrium and rate constants. The standard free energy of reaction 0 is 0.362 eV. Therefore, k_{-0} can be taken as equal to the diffusion limit (7.9×10^9 M^{-1} s^{-1}) and thus $k_0 = 4.75 \times 10^3$ M^{-1} s^{-1}. $K_1 = 9.9$ 10^{-5} M (from $\Delta G^0_{AHC(CH_3)_3^{\bullet+} \rightarrow AH^+ + (CH_3)_3^{\bullet}}$ in Table 1). Reactions 2 and 2′ have very large driving forces (0.910 and 0.548 eV, respectively). Their rate constants have thus been taken as equal to the diffusion limit. Once the working curves have been calculated the experimental values of i_p/i_p^0 at each scan rate can be used to determine the value of the dimensionless rate parameter for reaction 1, and thus of k_1, as shown by the arrows in Figure 5. Over the whole set of scan rate and concentration values, it was thus found that log $k_1 = 5.62 \pm 0.02$. The same experiments and data treatments were repeated with the same base, at two other concentrations, 10 and 90 mM, and with three

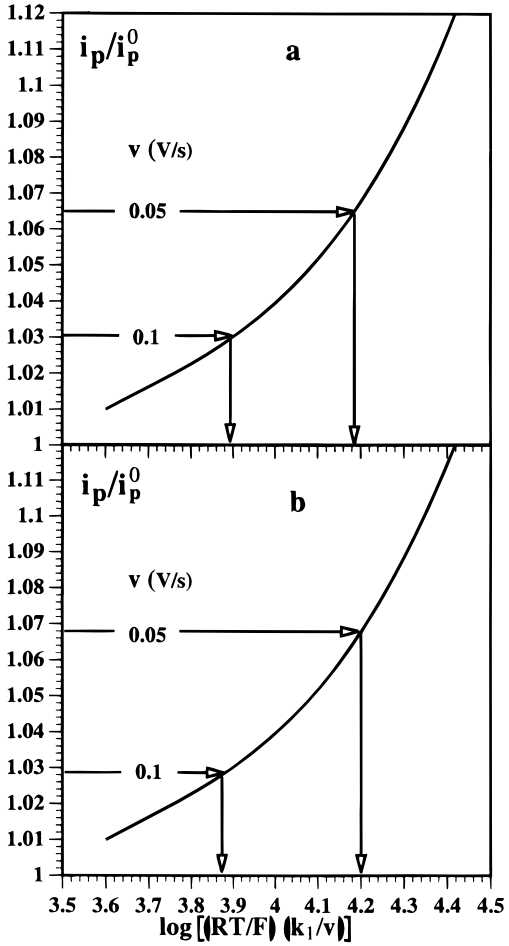

Figure 6. Cyclic voltammetry in acetonitrile + 0.1 M NEt_4BF_4 + 30 mM 3-fluoropyridine ($pK_a = 9.4$) of diacetylferrocene ($E^0_{cat} = 0.870$ V vs SCE) in the presence of $BQCNHC(CH_3)_3$. Variation of the normalized catalytic peak current with the dimensionless rate parameter of reaction 1 (see text) and determination of k_1 at various scan rates. [diacetylferrocene] = 3.16 (a) and 6.32 (b) mM. [$BQCNHC(CH_3)_3$] = 1.71 (a) and 3.42 (b) mM.

additional bases, 3-fluoropyridine ($pK_a = 9.4$), pyridine ($pK_a = 12.3$), 2,4,6-trimethylpyridine ($pK_a = 15.6$), at three concentrations, 10, 30, and 90 mM as well as with no base added. Over the whole series of conditions it was found that $\log k_1 = 5.6 \pm 0.15$.

With $BQCNHC(CH_3)_3$, diacetylferrocene ($E^0_{cat} = 0.870$ V vs SCE) was used as a catalyst. The decay of the cation radical is slower than in the preceding case leading to a smaller catalytic increase of the anodic peak. Figure 6 illustrates the determination of k_1 from the i_p/i_p^0 data along the same procedure. The standard free energy of reaction 0 is now 0.340 eV. Therefore, k_{-0} can again be taken as equal to the diffusion limit (7.9×10^9 M^{-1} s^{-1}), leading to $k_0 = 1.14 \times 10^4$ M^{-1} s^{-1}. Since $\Delta G^0_{AHC(CH_3)_3^{\cdot+} \rightarrow AH^+ + C(CH_3)_3^{\cdot}}$ (Table 1), $K_1 = 7.9 \times 10^{-6}$ M. Reactions 2 and 2′ still have very large driving forces (1.120 and 0.780 eV, respectively). Therefore their rate constants can be considered to be at the diffusion limit. From the data in Figure 6 it is thus found that $\log k_1 = 4.50 \pm 0.02$. The same experiments and data treatments were repeated with the same base, at two other concentrations, 10 and 90 mM, and with two additional bases, pyridine ($pK_a = 12.3$) and 2,4,6-trimethylpyridine ($pK_a = 15.6$), at three concentrations, 10, 30, and 90 mM as well as with no base added. Over the whole series of conditions it was found that $\log k_1 = 4.5 \pm 0.15$. We note that the two working curves in Figure 6a,b are practically the same. This is because the decay of the cation radical is relatively slow and therefore reaction 0 acts as a pre-equilibrium in front of the successive steps. In the case of $BQAHC(CH_3)_3$, there is a slight but significant difference between the two working curves in Figures 5a,b. This is due to the fact that, decay of the cation radical being faster, there is mixed kinetic control by reaction 0 and the successive steps.

Application of the redox catalysis method to $BNAHC(CH_3)_3$ requires particular care because decay of the cation radical is the fastest in the whole series and close to the upper limit of applicability of the method. Also, unlike the two preceding cases, the decay of the cation radical is too fast for $E^0_{AHC(CH_3)_3^{\cdot+}/AHC(CH_3)_3}$ to be derived from fast scan cyclic voltammetry. This parameter has thus to be determined within the redox catalysis method itself. Table 2 summarizes the experimental data obtained with two different catalysts, vinylferrocene and 4-nitrophenylferrocene. The following set of values was found to fit with all the experimental data as depicted in Table 2. $E^0_{BNAHC(CH_3)_3^{\cdot+}/BNAHC(CH_3)_3} = 0.85$ V vs SCE, $k_0 = 322$ M^{-1} s^{-1}, $k_{-0} = 7.9 \times 10^9$ M^{-1} s^{-1}, $K_1 = 0.01$ M, $k_1 = 4 \times 10^7$ s^{-1}, $k_{-1} = 4 \times 10^9$ M^{-1} s^{-1}, $k_2 = k_{2'} = 7.94 \times 10^9$ M^{-1} s^{-1}. In the conditions of experiment numbers 1 and 2, i_p/i_p^0 is rather insensitive to the characteristics of reaction 1 because reaction 0 is then the rate-determining step. Their main interest is thus that they allow the determination of $E^0_{BNAHC(CH_3)_3^{\cdot+}/BNAHC(CH_3)^{\cdot}}$. k_1 and K_1 were then derived from experiment number 3. In this experiment, the catalytic current has a plateau shape (Figure 7) instead of a peak shape due to the presence of a large concentration of substrate and to the fact that the cation radical decay is fast. In this case, fitting of the experimental data was carried out as depicted in Figure 7. Experiment number 4 served to confirm the validity of the preceding determinations using another catalyst (same parameter values as precedingly except $k_0 = 1.9 \times 10^4$ M^{-1} s^{-1}).

The decay rate constants of the various cation radicals are summarized in Figure 8.

Discussion

We see in Figure 8 that there is a strong acceleration of C−C fragmentation when going from A = MA to BQCN, BQA, and BNA (by *ca.* 6 orders of magnitude on total) as the thermodynamics go from very uphill to moderately uphill. It appears that the data points fall on a 1/(0.0582) V straight line corresponding to the following equation

$$\log k_1 = \log k'_{diff} - (F/RT)\Delta G^0$$

where k'_{dif} is the diffusion limited rate constant multiplied by 1 M. In other words, the reverse (bimolecular) coupling reaction is under diffusion control.

Although not always realized, the kinetics of a reaction that is monomolecular in the forward direction and bimolecular in the reverse direction, as is the present fragmentation of cation radicals, may be governed by the diffusion of the two products out of the solvent cage as depicted below.

$$A \underset{k_-^{act}}{\overset{k_+^{act}}{\rightleftharpoons}} (BC) \underset{k_{dif}}{\overset{k'_{dif}}{\rightleftharpoons}} B + C$$

Adaptation of the Debye−Schmoluchovski classical approach[21] for reactions that are bimolecular in both directions to the present case leads to the following equations.

$$k_+ = \frac{k'_{dif} k_+^{act}}{k'_{dif} + k'^{act}_-}$$

and

Table 2. Redox Catalytic Determination of the Decay Kinetics of $BNAHC(CH_3)_3^{\cdot+}$

expt no.	catalyst	E^0_{cat} (V vs SCE)	[cat] (mM)	[substrate] (mM)	scan rate (V/s)	i_p/i_p^0 theor	i_p/i_p^0 exptl
1[a]	vinylferrocene	0.420	2	1.04	0.1	1.16	1.15
					0.2	1.083	1.083
2[a]	vinylferrocene	0.420	8	4.2	0.1	1.39	1.37
					0.2	1.22	1.23
3[a,c]	vinylferrocene	0.420	8	33	0.1	3.08	3.04
					0.2	2.41	2.39
4[b]	4-nitrophenylferrocene	0.523	2	1	0.85	1.64	1.64
					1.65	1.45	1.40

[a] In acetonitrile + 0.1 M NEt_4BF_4 + 10 mM pyridine ($pK_a = 12.3$). [b] In acetonitrile + 0.1 M NEt_4BF_4 + 23 mM pyridine ($pK_a = 12.3$). [c] See Figure 7.

$$k_- = \frac{k_{dif}k'^{act}_-}{k'_{dif} + k'^{act}_-}$$

where k_{dif} is the bimolecular diffusion-limited rate constant and k'_{dif} is the first order rate constant obtained by multiplying k_{dif} by 1 M. k_+ and k_+^{act} are monomolecular rate constants, while k_- and k_-^{act} are bimolecular rate constants. k'^{act} is the first order rate constant obtained by multiplying k_-^{act} by 1 M. Thetwo equations above may equivalently be written as[21f]

$$k_+ = \frac{k_{dif}k_+^{act}}{k_{dif} + k_-^{act}}$$

and

$$k_- = \frac{k_{dif}k_-^{act}}{k_{dif} + k_-^{act}}$$

When the backward activation controlled reaction is faster than the diffusion of the two fragments out of the solvent cage, the overall rate constants becomes

$$k_+(s^{-1}) = k_{dif}(M^{-1}\,s^{-1})K(M) = k'_{dif}(s^{-1})\exp[-(F/RT)\Delta G^0]\;k_- = k_{dif} \quad (K = (k_+/k_-))$$

and where the first of these two equations corresponds to the line on which the data points fall in Figure 8.

Figure 9 shows two examples of mixed activation-diffusion control where activation has been assumed to follow a quadratic law as defined by the following equations

$$\Delta G_+^{\ddagger} = \Delta G_0^{\ddagger}\left(1 + \frac{\Delta G^0}{4\,\Delta G_0^{\ddagger}}\right)^2$$

with

$$k_+^{act} = \frac{kT}{h}\exp\left(-\frac{F\Delta G_+^{\ddagger}}{RT}\right)$$

($\Delta G_+^{\ddagger}$, activation free energy; ΔG^0, standard free energy of the reaction; $\Delta G_0^{\ddagger}$, intrinsic barrier free energy). It is seen that when the intrinsic barrier is small ($\Delta G_0^{\ddagger} = 0.2$ eV) the cleavage rate constant is controlled by the diffusion of the two fragments out of the solvent cage over the whole endergonic region as is the case with our cation radicals. The condition to be fulfilled for the reverse reaction to be under diffusion control is that its activation free energy is smaller than 0.18 eV.

Is there precedency to the kinetic behavior just described in cleavage reactions of ion radicals? In this connection, it is worth examining the kinetic data previously reported for C−C

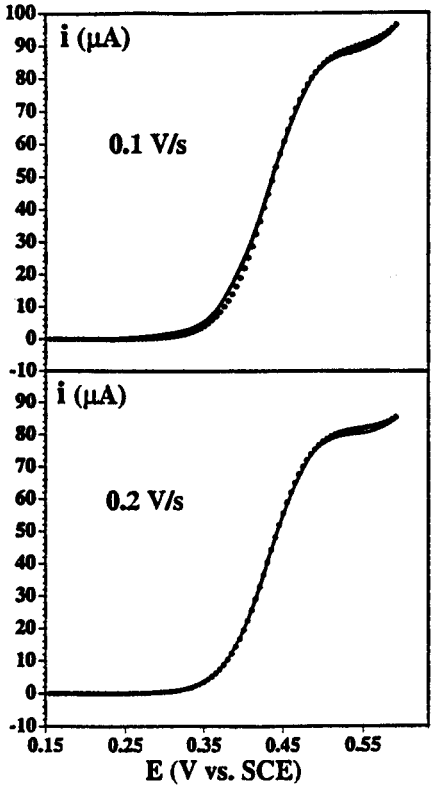

Figure 7. Cyclic voltammetry in acetonitrile + 0.1 M NEt_4BF_4 + 10 mM pyridine of vinylferrocene in the presence of $BNAHC(CH_3)_3$. Experiment number 3 (Table 2). Solid line: experimental curves, dots: simulated curves (see text).

(21) (a) von Smoluchowski, M. *Phys. Z.* **1916**, *17*, 557. (b) von Smoluchowski, M. *Phys. Z.* **1916**, *17*, 585. (c) von Smoluchowski, M. *Z. Phys. Chem.* **1917**, *92*, 129. (d) Debye, P. *Trans. Electrochem. Soc.* **1942**, *82*, 265. (e) Andrieux, C. P.; Savéant, J.-M. *J. Electroanal. Chem.* 1986, *205*, 43. (f) The Debye−Smoluchowski model of the interference of diffusion control in bimolecular reaction kinetics

$$A + C \underset{k_-}{\overset{k_+}{\rightleftharpoons}} B + D$$

treats the reactants as hard spheres and uses the Fick's law to describe the spherical diffusion of one of the reactant toward the other.[21a−e] It is equivalent to considering the following kinetic scheme

$$A + C \underset{k'_{dif}}{\overset{k_{dif}}{\rightleftharpoons}} (AC) \underset{k'^{act}_-}{\overset{k'^{+}_{act}}{\rightleftharpoons}} (BD) \underset{k_{dif}}{\overset{k'_{dif}}{\rightleftharpoons}} B + D$$

which also requires the introduction of pseudo-first order rate constants (noted k′) to obtain the expression of the overall rate constants

$$k_+ = \frac{k_{dif}k'^{act}_+}{k'_{dif} + k'^{act}_+ + k'^{act}_-} = \frac{k_{dif}k_+^{act}}{k_{dif} + k_+^{act} + k_-^{act}}$$

and

$$k_- = \frac{k_{dif}k'^{act}_-}{k'_{dif} + k'^{act}_+ + k'^{act}_-} = \frac{k_{dif}k_-^{act}}{k_{dif} + k_+^{act} + k_-^{act}}$$

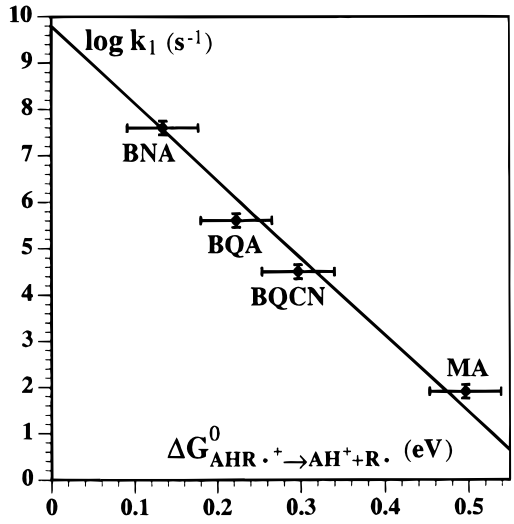

Figure 8. C−C fragmentation of $AHC(CH_3)_3$ cation radicals. Variation of the rate constant with the standard free energy of the reaction. Straight line: $\log k_1 = \log k'_{dif} - (F/RT)\Delta G^0$.

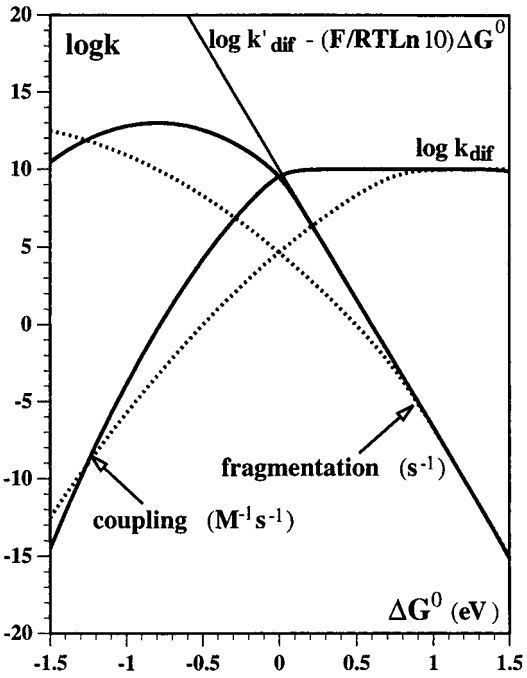

Figure 9. Example of Brönsted plots combining the effect of diffusion and of an activation obeying a quadratic law. Solid and dotted lines: $\Delta G_0^{\ddagger} = 0.2$ and 0.5 eV, respectively, $kT/h = 10^{13}$ s^{-1}, $k_{dif} = 10^{10}$ M^{-1} s^{-1}, $k'_{dif} = 10^{10}$ s^{-1}.

fragmentation in a remarkably extended series of bibenzyl cation and anion radicals bearing an electron-donating and an electron-withdrawing group respectively:[13f]

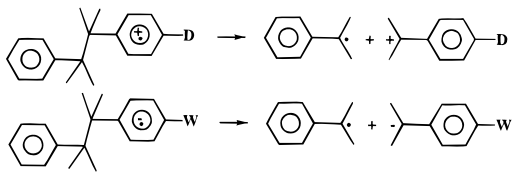

As seen in Figure 10, the data points corresponding to endergonic reactions fall nicely on the straight-line representing kinetic control by the diffusion of the two fragments out of the solvent cage. The three points (solid triangles) which correspond to ether as the solvent falls above the line as expected

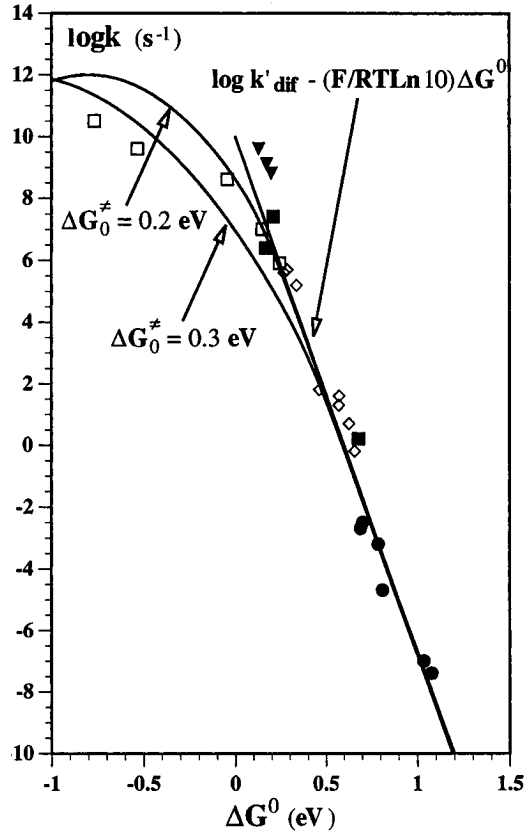

Figure 10. Cleavage rate constants of anion and cation radicals of substituted bibenzyls. ●, 1c−h; ◇, 2; □, 3, ▼, 4a−c; ■, 4d,e,5. Solvents: Me_2SO, CH_3CN, CH_2Cl_2/MeOH, PrCN/EtBr, CH_2Cl_2, MeOH, Et_2O (4a−c).

from the lower viscosity of this solvent compared to the others. In ref 13f, diffusion of the products out of the solvent cage was not taken into account as a possible rate-limiting factor. The reaction was assumed to be under activation control and the variation of the rate constant with the driving force was fitted with a quadratic relationship with a small intrinsic barrier free energy. The experimental results contained in ref 13 are described in more details in two publications that appeared after submission of the present paper.[22] Attempted correlations between the cleavage activation free energies of the ion radicals and of the parents should in fact be viewed as correlationsbetween the standard free energies of the two reactions resulting from the thermodynamic relationship

$$\Delta G^0_{AR\bullet_{-/+}\rightarrow A_{-/+}+R\bullet} = \Delta G^0_{AR\rightarrow A\bullet+R\bullet} +/- E^0_{AR\bullet_{-/+}/AR} -/+ E^0_{A_{-/+}/A\bullet}$$

This is also true for correlations with the strain energies and for solvents effects which should mostly influence the two standard potentials in the above equation.

Turning back to cation radicals of NADH analogues, it has been observed that $MAHCH_3^{\cdot+}$ and $MAHPh^{\cdot+}$ (as well as with their deuterated analogues) undergo deprotonation (or dedeuteration) rather than C−C fragmentation over the whole range of pH, unlike the *tert*-butyl derivatives.[9d] This behavior is related to the very poor driving force of C−C fragmentation for these two cation radicals. Estimation of $\Delta G^0_{AHR^{\cdot+}\rightarrow AH^{+}+R\cdot}$ along the same procedure as for the *tert*-butyl derivative leads to 0.888 and 1.352 eV, respectively. C−C fragmentation rate

(22) (a) Maslak, P.; Narvaez, J. N.; Vallombroso, T. M. *J. Am. Chem. Soc.* **1995**, *117*, 12373. (b) (a) Maslak, P.; Chapman, W. H.; Vallombroso, T. M.; Watson, B. A. *J. Am. Chem. Soc.* **1995**, *117*, 12380.

constants are thus predicted to be 4.4×10^{-5} and 4.7×10^{-14} s^{-1}, obviously unable to compete with deprotonation.

Conclusions

Cation radicals of *tert*-butylated NADH analogues, produced electrochemically or by reaction with homogeneous single electron acceptors, undergo C−C fragmentation rather than deprotonation. The reaction primarily yields AH^+ and the *tert*-butyl radical (and not $AH^{\cdot}$ and the *tert*-butyl cation). The potential required to produce the $AHC(CH_3)_3^{\cdot+}$ cation radical electrochemically is much more positive than the oxidation potential of the *tert*-butyl radical. Likewise, the standard potentials of the homogeneous single electron acceptors required to readily oxidize $AHC(CH_3)_3$ are much more positive than the oxidation potential of the *tert*-butyl radical. The *tert*-butyl radical initially formed is thus immediately oxidized to the *tert*-butyl cation which rapidly reacts with the solvent and/or residual water. The cation radical cleavage reaction is fast although endergonic in all four cases. Plotting of the fragmentation rate constants against the standard reaction free energies reveals that the reaction is kinetically controlled by the diffusion of the fragments out of the solvent cage rather than by activation parameters. This behavior implies that the intrinsic free energy is small (less than 0.2 eV) showing that internal and solvent reorganization energies are small. It is remarkable that the re-examination of the kinetic data previously reported for C−C fragmentation in an extended series of bibenzyl cation and anion radicals bearing an electron-donating and an electron-withdrawing group, respectively,[13f] indicates the same nature of the kinetic control in the endergonic region. In all these cases, the gathering of kinetic data does not provide insights on the nature and magnitude of the activation parameters but rather leads to the determination of the reaction thermodynamics. It is remarkable in this connection that the standard reaction free energies thus obtained agree so well with those derived indirectly by means of thermochemical cycles (note in this respect that, in Figure 8, the horizontal errors bars correspond to 1 kcal/mol).

Experimental Section

Chemicals. $MAHCH_2Ph$,[9d] $BNAHC(CH_3)_3$,[23] and $BQCNHC(CH_3)_3$[23] were prepared according to previously described procedures.

The new compound 1-benzyl-4-*tert*-butyl-3-carbamoyl-1,4-dihydroquinoline ($BQAHC(CH_3)_3$) was synthesized by addition of the Grignard reagent, $(CH_3)_3CMgCl$, to the benzylquinolinium salt $BQAH^+,Br^-$. The latter compound was prepared as described earlier.[24] A 2 M solution of $(CH_3)_3CMgCl$ (2.9 mL, i.e., 5.8 mmol) in diethyl ether was added dropwise to a stirred suspension of $BQAH^+,Br^-$ (1 g, 2.9 mmol) in 5 mL of dry tetrahydrofuran containing cuprous iodide (25 mg, 0.12 mmol) plus methyl sulfide (0.6 mL, 9 mmol) and maintained at 0 °C under argon. After 1 h, the mixture was stirred at 25 °C for another hour. Quenching of the mixture with 5% aqueous sodium hydrogenocarbonate (30 mL) precipitated salts and left a solution which was separated by decantation and extracted with diethyl ether (80 mL). After washing with water (3 × 80 mL), the organic solvent was removed under vacuum. The resulting residue was subjected to column chromatography on Merck basic alumina (70−230 mesh) eluted with 98−2 chloroform−methanol. The second eluted yellow band, corresponding to the crude product, was collected and subsequently purified by preparative HPLC on a Spherisorb ODS2 250 × 10.5 mm column (84−16 chloroform−methanol). Crystallization from ethanol/water gave a pure sample of 120 mg (13% yield) of pale yellow crystals: mp 187 ± 1 °C; ^{1}H NMR ($CDCl_3$) δ/ppm 7.65 (s, 1H), 7.42−7.02 (m, 8H), 6.88 (d, 1H, $J = 8.1$ Hz), 5.95 (bs, 2H), 4.90 and 4.92 (two innermost peaks, AB q, 2H, $J_{AB} = 16.7$ Hz), 3.65 (s, 1H), 0.86 (s, 9H); UV−vis, λ_{max}/nm (ϵ_{max}/M^{-1} cm^{-1}) in acetonitrile, 314 (11 370). Anal. Calcd for $C_{21}H_{24}N_2O$: C, 78.71; H, 7.55; N, 8.74. Found: C, 78.81; H, 7.54; N, 8.72.

For the synthesis of $MAHC(CH_3)_3$, we obtained a much better yield by addition of $(CH_3)_3CMgCl$ to MAH^+ than by photoreduction of MAH^+ in the presence of $(CH_3)_3CCOOH$ as described in the literature.[25] A 2 M solution of $(CH_3)_3CMgCl$ (9 mL, i.e., 18 mmol) in ether was added under argon to a stirred suspension of 10 mmol of MAH^+ in 10 mL of ether in an ice bath. The reaction mixture was stirred at 25 °C for *ca.* 20 min and then quenched with 40 mL of an aqueous 20% NH_4Cl solution. Filtration gave a precipitate which was extracted with ether. The ether extracts were combined and washed with water, and ether was evaporated under vacuum. $MAHC(CH_3)_3$ was isolated by flash column chromatography using 15 μm, grade 60 Merck silica gel (95−5 chloroform−hexane) and crystallization from ethanol/water, mp 112 °C ± 1. Characterization of the product (^{1}H NMR, elemental analysis) was consistent with that reported in ref 25.

All chemicals were obtained from Aldrich and were of the highest purity available. They were used as received with the exception of 1,1′-diacetylferrocene which was recrystallized from a 40−60 dichloromethane−hexane mixture.

Instruments and Procedures. They were the same as previously described for cyclic voltammetry, redox catalysis, laser flash photolysis, electrolysis and chromatography.[9,14a]

Controlled potential electrolyses of the various AHRs were carried out in deareated acetonitrile + 0.1 M *n*-Bu_4BF_4 (20 mL) containing an appropriate (see the Results section) concentration of base (50−200 mM). The working electrode was a platinum foil whose potential was set 100 mV beyond the cyclic voltammetric anodic peak potential. The AR^+ and AH^+ products were identified and quantified by comparison of their cyclic voltammetric anodic peaks with those of authentic samples. The conversion of the starting ARH was derived from the decrease of its cyclic voltammetric anodic peak current. In the case of $MAHC(CH_3)_3$, HPLC was also used to follow the course of electrolysis. Aliquots (20 μL) of the electrolyzed solution were injected into a reverse-phase Hypersil C_{18} ODS2 column. The mobile phases were (A) 80−20 methanol−water + 10 mM Na_2HPO_4 and (B) methanol. The gradient consisted of a 5 min isocratic step with 100% A, followed by a 7 min isocratic step with 100% B, and a 5 min linear step to initial conditions. The flow rate was 1.0 mL min^{-1}. The chromatrographic peaks were identified by UV at 290 and/or 342 nm by comparison with authentic samples. Quantitation of acridine (t_r = 5.4 min), MAH^+ ($t_r = 6.4$ min) and unreacted $MAHC(CH_3)_3$ ($t_r = 14.9$ min) was derived from integrated peak vs concentration calibration curves. HPLC was also used to analyze solutions of $MAHC(CH_3)_3$ (0.16 mM) + CCl_4 (0.1%) after irradiation of 1 mL solution with a 95 mJ laser pulse at 308 nm.

JA9542294

(23) Anne, A. *Heterocycles* 1992, *34*, 2331.
(24) (a) Shinkai, S.; Hamada, H.; Kusano, Y.; Manabe, O. *J. Chem. Soc. Perkin Trans. 2* **1979**, 699. (b) Anne, A.; Moiroux, J. *J. Org. Chem.* **1990**, *55*, 4608.
(25) Fukuzumi, S.; Kitano, T.; Tanaka, T. *Chem. Lett.* **1989**, 1231.